Effects on radiation oncology treatments involving various neuromodulation devices

Michael S. Gossman[a,*], Kunal J. Paralikar[b], Adam O. Hebb[c], Jeffrey D. Wilkinson[d],
Alison R. Graves-Calhoun[d], Raymond C. Lawson[a], Jeffrey P. Lopez[e] and James S. Powell[f]

[a]*Tri-State Regional Cancer Center, Radiation Oncology Department, 706 23rd Street, Ashland, KY, USA*
[b]*Medtronic, Inc., Neuromodulation Product Development and Technology RSE, 7000 Central Avenue NE, RCC160, Minneapolis, MN, USA*
[c]*University of Washington, Department of Neurological Surgery, 1959 NE Pacific, Box 356470, Seattle, WA, USA*
[d]*Medtronic, Inc., Rhythm Disease Management Division, External Research Program, 8200 Coral Sea Avenue MVN41, Mounds View, MN, USA*
[e]*Ashland Radiation Oncology, Radiation Oncology Department, 706 23rd Street, Ashland, KY, USA*
[f]*Tri-State Christian Neurosurgical Associates, Medical Plaza A, 617 23rd Street, Suite 15, Ashland, KY*

Abstract. *Object:* Where no society-based or manufacturer guidance on radiation limits to neuromodulation devices is available, this research provides the groundwork for neurosurgeons and radiation oncologists who rely on the computerized treatment plan clinically for cancer patients. The focus of the article is to characterize radiation parameters of attenuation and scatter when an incident therapeutic x-ray beam is directed upon them.

Methods: Ten neuromodulation models were chosen to represent the finite class of devices marketed by Medtronic before 2011. CT simulations permitted computer treatment modeling for dose distribution analysis as used routinely in radiation oncology for patients. Phantom case results were directly compared to actual clinical patient cases. Radiation detection measurements were then correlated to computational results. Where the x-ray beam passes through the device and is attenuated, dose reduction was identified with Varian Eclipse computer modeling for these posterior locations.

Results: Although the computer algorithm did not identify physical processes of side-scatter and back-scatter, these phenomena were proven by radiation measurement to occur. In general, the computer results underestimated the level of change seen by measurement.

Conclusions: For these implantable neurostimulators, the spread in dose changes were found to be −6.2% to −12.5% by attenuation, +1.7% to +3.8% by side-scatter, and +1.1% to +3.1% by back-scatter at 6 MV. At 18 MV, these findings were observed to be −1.4% to −7.0% by attenuation, +1.8% to 5.7% by side-scatter, and 0.8% to 2.7% by back-scatter. No pattern for the behavior of these phenomena was deduced to be a direct consequence of device size. At the time of this writing, manufacturers of Neuromodulation products do not recommend direct exposure of the device in the beam nor provide guidance for the maximum dose for these devices.

Keywords: Accelerator, Medtronic, neuromodulation, neurostimulator, oncology, radiation

*Corresponding author: Michael S. Gossman, M.S., DABR, Tri-State Regional Cancer Center, Radiation Oncology Department, 706 23rd Street, Ashland, Kentucky 41101 USA. Tel.: +1 606 329 0060; Fax: +1 606 325 9366; E-mail: mgossman@tsrcc.com.

1. Introduction

Neuromodulation is becoming an increasingly popular clinical tool to alleviate symptoms of various neurological challenges, including chronic pain, urinary incontinence, and movement disorders. The target structure for Neuromodulation within the central or peripheral nervous system is determined by the particular application. A neuromodulation system typically consists of an implantable neurostimulator or pump, and at least one electrode array or catheter. The broad scope and acceptance for neuromodulation may create issues for the radiation oncologist and the neurosurgeon when their patient is diagnosed with a cancer requiring radiation therapy after a device has already been implanted. The surgical removal and re-implantantation increases the likelihood of infection, increases the medical cost due new device purchase, and creates a considerable loss of therapy time [1–4]. Consequences of device removal may include a return of the patient's symptom for which it was originally implanted [3]. Specialized surgeries such as these also come with a risk in detrimental effects, such as infection, hematomas or seromas in the area where the device is implanted. Repeating surgeries are cost burdening and time inefficient as well. Even to the FDA, these are valid concerns even for relocating the device or minimizing exposure to it [5].

It is likewise a quandary for the radiation oncologist specifically to consider the effects of having the device in the field of radiation. Unlike some heart rhythm devices, the maximum allowed dose for these neuromodulation devices is not available from any manufacturer nor have test results been published by researchers. Therefore, a recommendation to "not place the device directly in the field of radiation" is provided, which is expected to be considered when planning radiotherapy procedures [6]. This creates difficulty in targeting the disease of concern. Examples of such situations are when the tumor is in lungs or near the abdomen with the device implanted in the sub-clavicular region or abdomen or when the tumor is in the brain or spinal cord with the electrode implanted in close proximity. Although a single deep brain stimulator is routinely implanted in the recipient, at times a bilateral pectoral implant may be required in the rare case. Radiation therapy delivery for breast and lung then become particularly problematic, since there is not just one device obstacle, but bilateral obstacles. Particle accelerator beam angle adjustments can compensate to some degree to avoid the device and still target the tumor in most cases, however, the optimum angle may not be entirely or acceptably achievable. An unsatisfactory conclusion may be that either the tumor will be inadequately covered by the dose distribution intended or the unknown beam blocking effect will reduce dose significantly at the tumor [7].

At the root of these issues is the concern over the inaccuracy of the computerized modeling depended upon by the radiation oncologist to make these decisions. Medical physicists have published on such modeling inaccuracies for mandibular bridging plates, hip prosthetics, vascular access ports, and most recently pacemakers and cardioverter-defibrillators with remarkable variances of well over 10% in contrast to radiation measurements [8–11]. This research aims to assist the neurosurgeon, radiation oncologist and medical physicist involved in the consideration of such an impasse during the external beam radiation therapy treatment planning process. Ten marketed neuromodulation devices for analysis have been acquired. Computerized tomography scans were conducted on the devices and leads in a liquid water phantom setting. Then each scan was sent to a treatment planning computer for simulation. Radiation measurements followed and compared to the modeling results. Case studies are presented additionally, with dosimetry local to where the device or electrode leads were implanted. From this research, we promulgate this American Association of Physicists in Medicine (AAPM) requested and required information associated with effect of device on radiation beam lacking in literature for the radiation therapy team to consider [12].

Table 1
Medtronic neuromodulation device and lead information

Generator	Information
Itrel 3, Synergy Versitrel, Restore Advanced, Prime Advanced, Restore Ultra	Spinal Cord Stimulator
Soletra, Kinetra	Deep Brain Stimulator
Synchromed II	Drug Pump
InterStim II	Sacral Nerve Stimulator
Enterra	Gastric Stimulator
3777	Percutaneous Lead
3387	DBS Lead
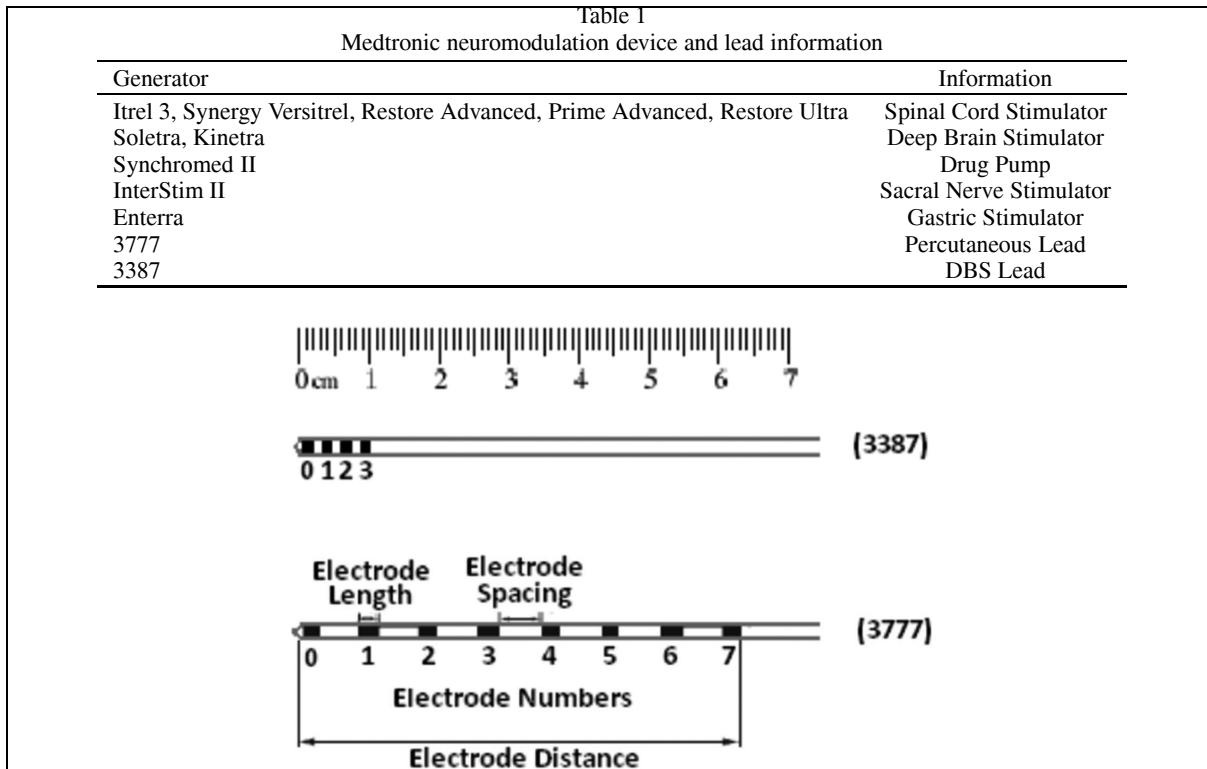
Fig. 1. Medtronic neurostimulation electrode lead drawings. Scale is 1.0 cm; electrode lead model 3387 and model 3777.

2. Materials and methods

2.1. CT scan acquisition

This research involves only Medtronic marketed neuromodulation devices and few electrode leads. Stimulation leads incorporated into the study include model 3777 and model 3387. Figure 1 shows the two electrode lead models used. Figure 2 provides a photograph of the various devices under investigation. Table 1 summarizes the device indications.

The test phantom geometry for conducting a computerized tomography (CT) scan of the devices and leads were created in a CNMC Company, Inc. (Nashville, TN) Model WP-3040 water phantom. Transparent acrylic plates were positioned at the bottom of the tank to provide a level platform for the devices during scanning. These also adequately insured back-scatter build-up with an 8.0 cm total thickness. The tank was then filled with water to a depth of 12.3 cm, insuring 4.3 cm of water above the top of the acrylic platform positioned inside. This depth was sufficient to achieve a necessary build-up of dose for both the 6 MV and 18 MV therapeutic x-ray energies, which occurs clinically at 1.5 cm and 3.0 cm respectively. The selected device was then centered and adhesively affixed to the acrylic top plate in the phantom.

The scan acquisition data for the CT imaging was obtained using a General Electric (Fairfield, CT) LightSpeed RT^{TM} scanner. A helical model stereotactic radiosurgery protocol was used, which included a 120 kVp x-ray beam operating on average at 198 mA. Couch increments provided for images at 1.25 mm/slice. The largest field of view at 50 cm was utilized. Following all 10 scans, all data sets

Fig. 2. Medtronic neurostimulation device illustration. Scale is 1.0 cm: At center top down – InterStim II model 3058 and Synchromed II model 8637-40; Clockwise – Enterra model 3116, Kinetra model 7428, Restore Advanced model 37713, Itrel 3 model 3387, Restore Ultra model 37712, Prime Advanced model 37702, Synergy Versitrel model 7427V, and Soletra model 7426. (Colours are visible in the online version of the article; http://dx.doi.org/10.3233/XST-2011-0306)

totaling 2,536 images were auto-generated using a commissioned extended Hounsfield unit CT range and sent to the treatment planning computer.

As published for deep brain neuromodulation lead localization techniques, the extended HU ranges were important for the observance of high density materials for sub-millimeter positioning accuracy in neurosurgery [13,14]. It is likewise used for proper computerized dose estimations in radiation oncology, which have been specifically addressed for metal devices such as implantable pacemakers, cardioverter-defibrillators, and vascular access ports [10,11]. The default range for the GE Lightspeed RT^{TM} scanner is $-1,024$ to $+3,071$ HU. This differs substantially from its extended range of $-31,743$ to $+31,743$ HU. Prior published studies have shown that high density metals such as titanium and stainless steel at nearly $+8,000$ HU and $+12,000$ HU respectively [10,11,13]. With the HU value being a determining factor in the computation of simulated dose, from which medical physicists and radiation oncologists approve treatment, it is important to not only be able to image for HU accuracy, but for dose estimation accuracy.

Two clinical cases were identified as relevant to this research endeavor and are presentation in this paper. The first clinical CT series was a chest scan from a patient diagnosed with a left-sided breast cancer, shown in Fig. 3. For this case, a helical model CT scan was acquired with a technique of 120 kVp at 196 mA and couch increment 5.0 mm/slice. The largest field of view at 50 cm was utilized. All 63 images were auto-generated using the commissioned extended Hounsfield unit CT range. Axial images
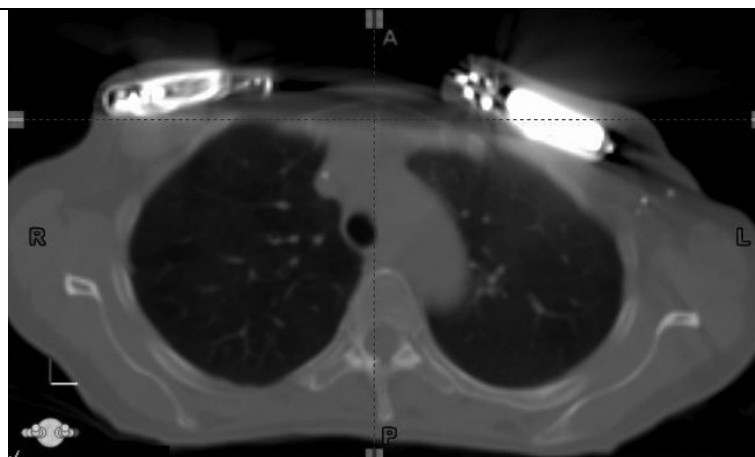
Fig. 3. Clinical Case: Medtronic deep brain stimulators Soletra (patient's right side) and Kinetra (patient's left side) – Orientation feet first & supine. (Colours are visible in the online version of the article; http://dx.doi.org/10.3233/XST-2011-0306)

delineated the presence of devices positioned bilaterally on each chest wall. Operational notes revealed the patient had been previously implanted with a deep brain stimulator on both sides, with a Soletra on the right side and a Kinetra on the left side. Electrode lead model 3387 was discovered to be connected to the device, but not visible in the chest scan shown in Fig. 3.

The second clinical CT series was a brain scan from a patient diagnosed with advanced Parkinson's disease [14]. Management was arranged by the neurosurgeon with the use of a Kinetra deep brain stimulator using two identical model 3387 leads shown in Fig. 4. The helical brain scan was performed on a General Electric VCT 64 detector system. Inherent extended Hounsfield unit range scan acquisition was included and maintained throughout reformatting. The technique was 140 kVp at 600 mA at couch increment 0.6 mm/slice. A field of view at 25 cm was utilized. All 251 unmodified images were manually generated from the conversion of Digital Imaging and Communications in Medicine (DICOM) standard image files to the Neuroimaging Informatics Technology Initiative (NIFTI-1) (National Institute of Mental Health; National Institute of Neurological Disorders and Stroke, Bethesda, MD) format using a Statistical Parametric Mapping (SPM5) (Welcome Trust Centre for Neuroimaging, London) software platform. This series was then sent to the treatment planning computer.

2.2. Dose computation

Computerized dose modeling for radiation oncology simulation use was performed using the Varian Medical Systems, Inc. (Palo Alto, CA) Eclipse software build version 8.6.17. Once all scan sets were imported, every slice was reviewed for artifacts. Discrepancies in image data appeared as expected in the vicinity of material with high atomic number [10,11]. Improper sampling of data from kilovoltage x-ray beam hardening result in false attenuation and thus incorrect Hounsfield units. The findings of streak artifacts exhibited laterally in each scan were evidence of this phenomenon. An incorrect assignment of HU values for materials in the scan may result in incorrect dose computation. However, techniques are described here to suitably remove these disturbances and causes of calculation inaccuracy.

The artifacts in the image were local to the position of the device. Erroneous values in water near the device register up to 5,800 HU, where it should be within $\pm$ 50 HU. Knowing that the phantom is entirely constructed with water-equivalent media, with the exception of the metal device, all Hounsfield

Table 2
Medtronic INS model dimensions

Generator	Model	L (cm)	W (cm)	T (cm)	V (cm3)
Synchromed II	8637–40	7.2	8.8	2.0	126.7
Kinetra	7428	6.1	7.6	1.3	60.3
Restore Advanced	37713	6.5	4.9	1.5	47.8
Prime Advanced	37702	6.5	4.9	1.5	47.8
Synergy Versitrel	7427V	5.8	5.6	1.3	42.2
Enterra	3116	5.5	6.0	1.0	33.0
Soletra	7426	5.5	6.0	1.0	33.0
Itrel 3	3387	5.5	6.0	1.0	33.0
Restore Ultra	37712	5.4	5.4	0.9	26.2
InterStim II	3058	5.1	4.3	0.8	17.5

Fig. 4. Clinical Case: Medtronic electrode lead models 3387 – Orientation head first and supine in the digitally reconstructed radiograph.

units around the device should be the defined reference water value. Therefore, artifacts were removed and their consequential impact to dosimetry negated by assigning a fixed value of 0 HU around it. Boolean operation satisfied this need. The size of the neurostimulation devices have been provided by the manufacturer as shown in Table 2 sorted by size [6]. Using these dimensions, the Eclipse software was used to contour the devices in each scan set. A duplicate structure was then created, superimposed on the original device contour, and expanded in three dimensions by a few centimeters. A Boolean operator was then used to subtract the volume of the device from the expanded volume. The process results in a contoured volumetric structure that completely envelopes the device, but does not include the device, and contains no artifact data.

The 3D absorbed dose computation was performed using the Varian Medical Systems, Inc. Anisotropic Analytical Algorithm version 8.6.15. It integrates measured radiation data from a Varian Medical Systems, Inc. model 21EX (Trilogy modified) particle accelerator, and is capable of using manually manipulation of beam geometries for simulating targeted dose with modulated, respiratory phase-gated,

and stereotactic deliveries with the most accurate results [15]. In accordance with standards from the AAPM Task Group No. 51, the particle accelerator was calibrated for 6 MV and 18 MV x-rays, to a dose of 1.00 cGy per monitor unit at the water depth resulting in maximum depth dose measurement [16]. Again, these build-up dose depths were clinically achieved at 1.5 cm for 6 MV and 3.0 cm for 18 MV.

Manual treatment plan modeling for the phantom began with the assignment of a single anterior field defined by a flat and symmetric 40×40 cm^2 beam size. The central axis of the beam passed directly through the center of the device. The gantry angle was adjusted to insure the central axis was perpendicular to the anterior face of the device. The rotational center of the accelerator was set to be at anterior face of the acrylic plates, which correspond to the posterior side of the device. The reference point location for programming the algorithm to prescribe dose was insured to be identically set at 2.4 cm, at or beyond the maximum depth dose. Since it is inappropriate to set the prescription point in the center of a high density device, invalid dose simulations were avoided by assigning the final position of the reference point to be off-axis from the central ray by a minimum of 8.0 cm in both axes. The smallest possible dose calculation grid of 0.20 mm was assigned. As an alternative to assigning fixed monitor units during calculation, we used the quotient of resulting monitor units to the resulting point dose to remove calculation deviations.

For the clinical case involving the Soletra and Kinetra only, an additional virtual compensator composed of water density was added to the body contour outline of the patient, with thickness 1.0 cm. This was done to negate computerized modeling inaccuracies in calculations that occur in the build-up region of the x-ray beam, since the devices were implanted superficially. For the clinical brain case involving the two identical model 3387 electrode leads, the depth from the skin to the leads is also appreciatively deep enough to insure therapeutic dose build-up. The additional compensator contour is unnecessary for the any of the 10 water phantom tests, since adequate water depth to the face of the device or lead was insured.

Programming was completed with a prescription of 100 cGy tied to the reference point. The treatment planning computer then determined the time for irradiation necessary to achieve the dose at that point. Note that this calculation was performed separately for the two DBS devices, so that no cumulative effect resulted to either of the bilaterally placed devices. For this clinical case specifically, results were gathered specifically for each device exclusively of any contralateral beam contribution. After the computer system computed the necessary beam-on time, it convolved a 3D dose distribution showing isodose lines throughout the phantom volume.

The change in the depth and percentage level of the isodose lines from normal scans of water in the absence of any such device detail the effect of having an implantable device in the field of radiation. In order to directly make such a comparison, a baseline treatment plan was created. By copying the plan and reassigning all structures in the scan to have unit density (0 HU), the computation was performed with the algorithm assuming only water density for the entire phantom environment.

For the devices, calculation points of interest were positioned strategically where maximum changes were observed in review of the shape of isodose lines in the heterogeneous plan. Anterior point placement was at 0.5 cm. Lateral point placement was assigned at 0.5 cm. Posterior point placement was registered at 0.5 cm and 2.0 cm distances. Each calculation point of interest was measured from the surface of the contoured device. It was not expected that scatter changes be discernable for the electrode leads. However, calculation points were placed in each of those plans for an attenuation result. Points were placed anterior and posterior from the center-most aspect of the electrode tip at 0.5 cm. Points placed posterior to the conducting wire leading up to the electrode were at 0.5 cm.

Then, calculation points were assigned at the identical coordinates in the homogeneous plan for comparison. The ratio of point-dose between the heterogeneous plan and the homogeneous plan provide

the level of affect each implantable device had on the therapeutic beam. The analysis method is consistent with published guidance of AAPM Task Group No. 63 for simulating dose involving high atomic number materials in radiation oncology [17]. The routine of creating heterogeneous and homogeneous plans with selective point placement was conducted for the separate phantom cases described as well as for the clinical chest cases involving the Soletra, Kinetra, and electrode lead model 3387 in the brain. Each was studied at 6 MV and 18 MV x-ray energies. The dose resulting at each point was compared between plans to yield the overall dose change effects.

2.3. Radiation measurements

Physical radiation measurements of scatter from neurostimulation devices were performed in the same geometry as simulated. Making use of the WP-3040 water tank, water was filled to a depth of 12.3 cm, insuring 4.3 cm of water above the top of the 8.0 cm Platform positioned inside. Scatter output readings were acquired using a CNMC Company, Inc. model 206 electrometer with charge range element model 206–110. The electrometer was connected to a Wellhofer-Scanditronix Farmer-type ionization chamber model TN31014 with sensitive volume $0.015\,cm^3$ and equilibrated to nominally +300 V at the center-pin. Using a 0.5 cm piece of water-equivalent rubber to assist with spacing, the "pin-point" chamber was adhesively affixed to a distance of 0.5 cm anterior to the face of the device above the device side as indicated by simulation to be the primary location of largest dose gradients. Again, with the isocenter of the particle accelerator verified by lasers to be at the posterior side of the device, a single $40 \times 40\,cm^2$ anterior field was programmed and delivered for 100 monitor units (15 sec) at a rate of 400 cGy/min. Charge was collected in a set of repeated measurements by the electrometer during delivery. Side scatter was conducted for all devices similarly, at 0.5 cm away.

Ionization readings were then collected for electrode lead model 3777. The same geometry was engaged for these measurements. The water in the tank was maintained at a depth of 4.3 cm. The attenuation measurements were achieved using the thimble chamber at 0.5 cm posterior from the center of the electrode tip. Identically as for the neuromodulation device, measurements were taken with the electrode lead model 3777 in place, and then repeated with it removed.

The phantom used for attenuation measurements by neuromodulation devices was a homemade glass phantom with a square area of $30 \times 30\,cm^2$, base thickness 0.3 mm and height 22.5 cm. Each INS was consecutively placed at the bottom of the phantom. Water was then added similarly as before, resulting in 4.3 cm water depth. This phantom geometry permitted radiation measurements to be acquired using a Sun Nuclear (Melbourne, FL) MapCheck diode array with software version 5.00.00. The detector system included 445 diodes embedded in a water equivalent plastic at a depth of 2.0 cm beneath the surface in a plane $22 \times 22\,cm^2$ in area. Radiation dose measurements were taken posterior to the bulky device. As used in planning, the measurement was taken at a distance 2.0 cm away, although with a detector limiting field size of $20 \times 20\,cm^2$. Measurements were then made without the neuromodulation device included. The software has the capability of plotting the dose from two plans in any one particular plane. Where isodose distribution changes are seen for the beam profiles between heterogeneous and homogeneous plans, a resulting subtraction plot makes known all the notable shifts in dose between measurements with and without the stimulator submerged. This gives rise to the affect of a device being in the radiation beam. Radiation measurement results were then correlated with the treatment planning system simulations. Both detector setup illustrations are shown in Fig. 5. All radiation measurements were conducted at 6 MV and 18 MV energies on the Varian model 21EX particle accelerator. Results were analyzed for percentage change as determined from data with and without the device included in
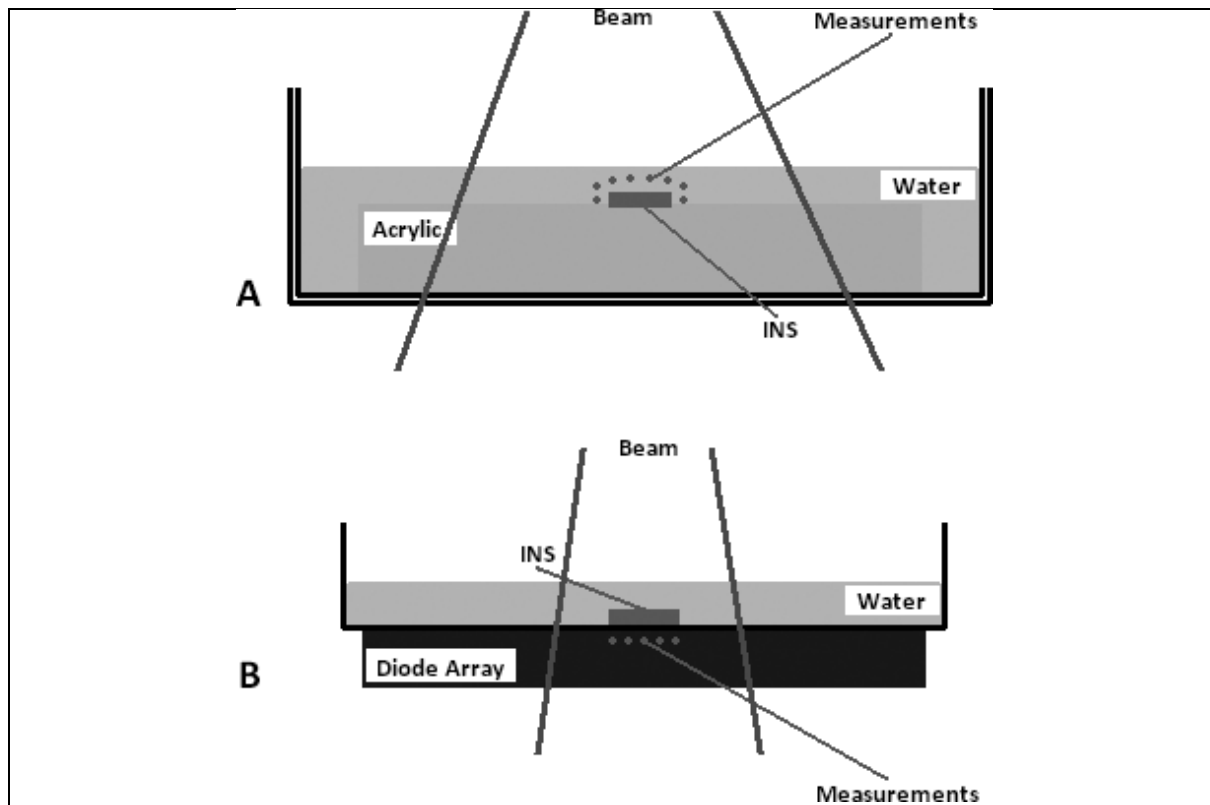
Fig. 5. Setup for radiation measurements, (A) side-scattering and back-scattering with miniature ionization chamber, (B) attenuation with diode array. (Colours are visible in the online version of the article; http://dx.doi.org/10.3233/XST-2011-0306)

the water medium. These results were then compared to the outcome of computerized dose simulation changes. Conclusions were generalized based on the complex dose modeling and strategic radiation measurements.

3. Results

Figure 5 offers an illustration of CT scan geometry used for simulation modeling. The dose distributions are shown surrounding the electrode leads in the phantom. For the clinical chest case involving the two stimulator devices, the distribution of dose is shown in Fig. 6. The results of the treatment planning simulations are shown in Tables 3 and 4, separated according to x-ray energy. The greatest dose gradients were observed for the Synergy Versitrel models at both 6 MV and 18 MV x-rays. The dose distributions in the axial and sagittal planes are presented in Fig. 7. Similarly, the distributions of dose for the Kinetra and Soletra in the clinical case are shown in Fig. 8.

4. Conclusions

The observance of high levels of attenuation identified through computer modeling was validated by radiation measurements. At 6 MV, attenuation ranged from -6.2% (Interstim II) to -12.5% (Syncromed

Table 3
Maximum dose change results for interaction processes simulated on computer and measured at 6 MV

Device	Simulated			Measured			Δ (Measured − Simulated)		
	Atten (2 cm)	Side-scatt (0.5 cm)	Back-scatt (0.5 cm)	Atten (2 cm)	Side-scatt (0.5 cm)	Back-scatt (0.5 cm)	Atten (2 cm)	Side-scatt (0.5 cm)	Back-scatt (0.5 cm)
Synchromed II	−7.9%	1.8%	0.4%	−12.5%	3.8%	3.1%	−4.6%	2.0%	2.7%
Kinetra	−9.3%	2.4%	0.6%	−9.5%	2.7%	2.4%	−0.2%	0.3%	1.8%
Kinetra (pt. case)	−6.1%	0.0%	−0.1%	−	−	−	−	−	−
Restore Advanced	−7.7%	0.3%	−0.1%	−10.7%	3.0%	2.1%	−3.0%	2.7%	2.2%
Prime Advanced	−5.3%	−0.1%	0.0%	−9.8%	3.1%	2.0%	−4.5%	3.2%	2.0%
Synergy Versitrel	−11.3%	2.3%	0.2%	−9.2%	2.6%	1.8%	2.1%	0.3%	1.6%
Enterra	−4.9%	−0.1%	−0.1%	−10.8%	3.0%	2.4%	−5.9%	3.1%	2.5%
Soletra	−3.7%	−0.2%	−0.1%	−7.5%	2.1%	1.7%	−3.8%	2.3%	1.8%
Soletra (pt. case)	−8.6%	1.9%	0.0%	−	−	−	−	−	−
Itrel 3	−4.7%	−0.7%	−0.4%	−8.8%	2.5%	2.2%	−4.1%	3.2%	2.6%
Restore Ultra	−7.0%	1.4%	0.4%	−8.7%	2.4%	1.7%	−1.7%	1.0%	1.3%
InterStim II	−3.0%	−0.2%	0.2%	−6.2%	1.7%	1.1%	−3.2%	1.9%	0.9%
Electrode lead 3777	−0.9%	0.0%	0.0%	−4.2%	0.0%	0.0%	−3.3%	0.0%	0.0%
Electrode lead 3387	−2.9%	0.0%	0.0%	−	−	−	−	−	−
Electrode lead 3387 (pt. case)	−3.6%	0.0%	0.0%	−	−	−	−	−	−
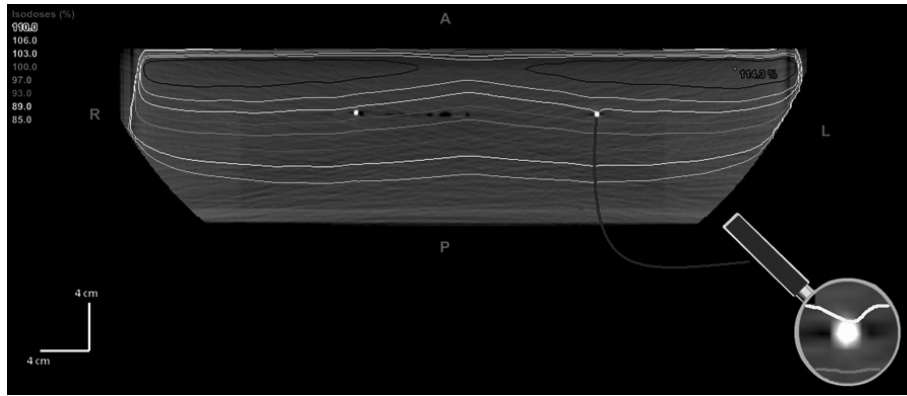
Fig. 6. Heterogeneous phantom density dose distribution in the axial view from 6 MV x-rays on Medtronic electrode lead model 3777 (used with Itrel 3 spinal cord stimulator) – Orientation head first and supine. (Colours are visible in the online version of the article; http://dx.doi.org/10.3233/XST-2011-0306)

II). At 18 MV, attenuation levels decreased to −1.7% (Interstim II) to −7.0% (Syncromed II). Attenuation results were consistent with nearly the same device ranking from greatest dose change to the least. No deduced pattern for the behavior of these phenomena was made possible with respect to device size; even though the Syncromed II pump had more than twice the volume of all the other devices and presented the greatest change in dose. Smaller devices such as the 33.0 cm^3 Enterra model showed greater attenuation at 6 MV than the larger 60.3 cm^3 Kinetra and 47.8 cm^3 Restore Advanced models.

There was no focus directed toward effects made possible as a consequence electrodes remaining in the beam. Rather, results were followed for completeness in this research. Some attenuation was observed for electrode lead model 3777. At 6 MV, the electrode tip was found to block radiation by −4.2%. At 18 MV, this affect was lessened to −3.1%. Electrode lead model 3387 was only simulated for dose alteration.

While attenuation decreased the output, scattering processes were found to increase dose for all devices and all energies. Positive scattering results reflect additional dose measured at the detector when the INS

Table 4
Maximum dose change results for interaction processes simulated on computer and measured at 18 MV

Device	Simulated			Measured			Δ (Measured − Simulated)		
	Atten (2 cm)	Side-scatt (0.5 cm)	Back-scatt (0.5 cm)	Atten (2 cm)	Side-scatt (0.5 cm)	Back-scatt (0.5 cm)	Atten (2 cm)	Side-scatt (0.5 cm)	Back-scatt (0.5 cm)
Synchromed II	−5.1%	2.2%	1.9%	−7.0%	4.4%	1.9%	−1.9%	2.2%	0.0%
Kinetra	−6.1%	3.0%	2.5%	−4.4%	3.0%	2.5%	1.7%	0.0%	0.0%
Kinetra (pt. case)	−4.7%	0.0%	0.0%	−	−	−	−	−	−
Restore Advanced	−4.8%	0.4%	0.3%	−4.2%	3.4%	2.4%	0.6%	3.0%	2.1%
Prime Advanced	−3.5%	−0.1%	−0.1%	−5.0%	5.0%	2.1%	−1.5%	5.1%	2.2%
Synergy Versitrel	−7.3%	2.8%	2.4%	−4.2%	4.2%	1.8%	3.1%	1.4%	−0.6%
Enterra	−3.2%	−0.1%	−0.1%	−1.4%	1.8%	0.8%	1.8%	1.9%	0.9%
Soletra	−2.5%	−0.2%	−0.2%	−4.4%	4.2%	1.9%	−1.9%	4.4%	2.1%
Soletra (pt. case)	−3.3%	0.1%	0.0%	−	−	−	−	−	−
Itrel 3	−3.1%	0.7%	0.0%	−5.4%	5.7%	2.7%	−2.3%	5.0%	2.7%
Restore Ultra	−4.6%	1.7%	1.5%	−4.9%	4.2%	2.4%	−0.3%	2.5%	0.9%
InterStim II	−1.9%	−0.2%	−0.2%	−3.8%	3.0%	2.4%	−1.9%	3.2%	2.6%
Electrode lead 3777	−0.2%	0.0%	0.0%	−3.1%	0.0%	0.0%	−2.9%	0.0%	0.0%
Electrode lead 3387	−0.9%	0.0%	0.0%	−	−	−	−	−	−
Electrode lead 3387 (pt. case)	−1.9%	0.0%	0.0%	−	−	−	−	−	−
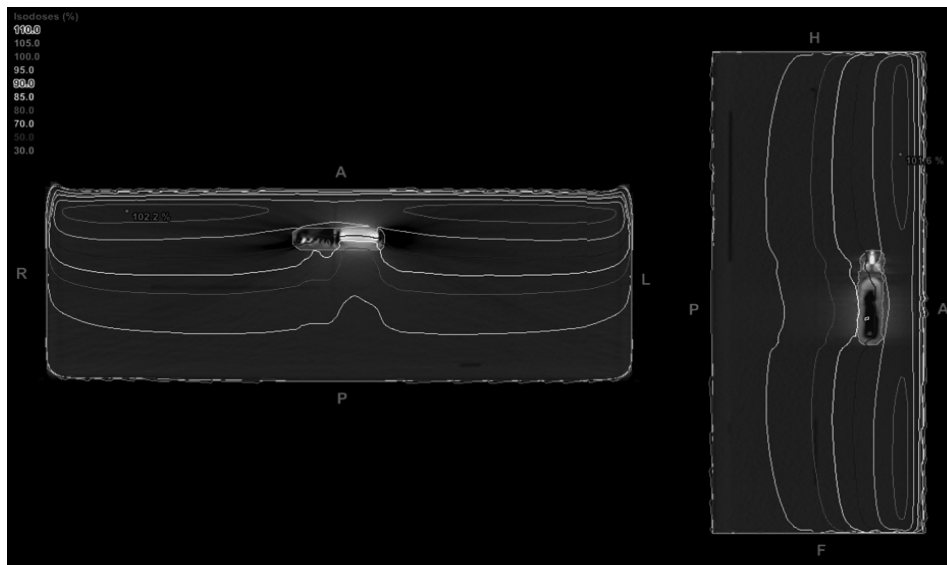
Fig. 7. Heterogeneous phantom density dose distribution from 6 MV x-rays on Medtronic Synergy Versitrel neuromodulation device in the axial view (left) and sagittal view (right). (Colours are visible in the online version of the article; http://dx.doi.org/10.3233/XST-2011-0306)

device was in position. At 6 MV, the magnitude of side-scatter and back-scatter occur at about 25% and 20% of the attenuation value respectively. The interaction cross-section was determined to increase with respect to incident photon energy. At 18 MV, side-scatter and back-scatter occurred roughly to 80% and 40% of the attenuation value. Measurements conclude that side-scatter radiation presents a greater level of change than back-scattering for all devices and all energies. Again, no deduced pattern for the behavior of these phenomena was made possible with respect to device size. It is then inferred that scattering events are more of a consequence of device construction. For the entire data set, side-scattering was measured to be less than 5.0%, with back-scattering found to be 3.1% at most.
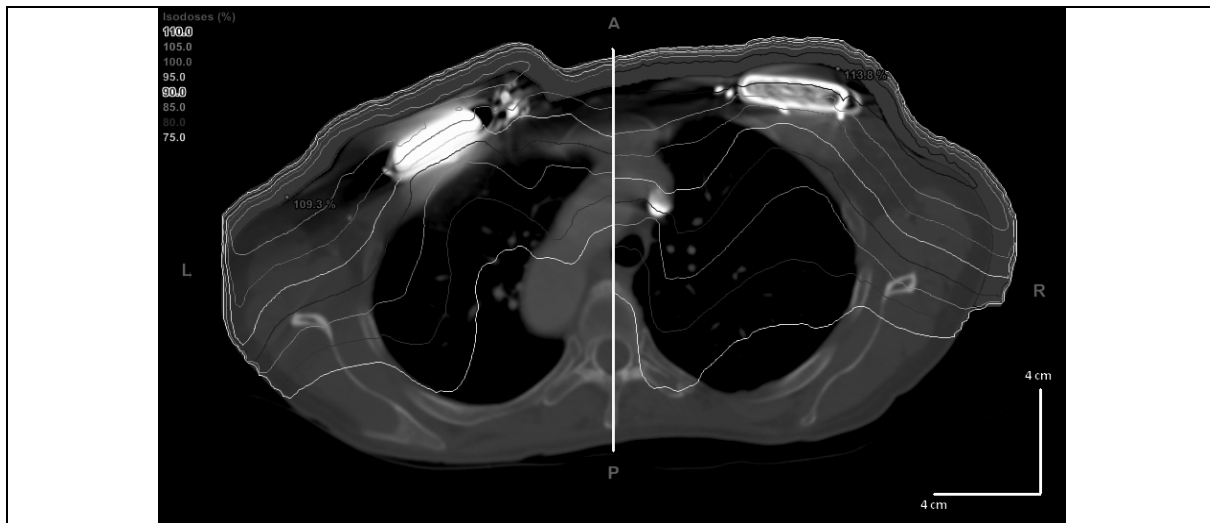
Fig. 8. Clinical Case: Heterogeneous density dose distribution in the axial view from 6 MV x-rays on Medtronic deep brain stimulators Soletra (patient's right side) and Kinetra (patient's left side) – Orientation feet first and supine. (Colours are visible in the online version of the article; http://dx.doi.org/10.3233/XST-2011-0306)

The treatment planning software was expected to have good fidelity for enhancement/attenuation in volumes with millimeter inhomogeneities, although it was found to underestimate attenuation and scatter processes considerably at both x-ray energies when modeling highly metallic neurostimulation devices. We have shown how computer inaccuracy can impact the judgment of acceptable dose distributions in association with cancer treatment. Using these simulated results and with the computers verified by radiation measurements, radiation oncologists and neurosurgeons may then understand the lack of accuracy seen in computer treatment planning systems in this regard, the magnitude of dose changes exhibited by neurostimulation devices when fully calculated, and the percentage level these processes occur in relation to the proximity of the device.

No recommendations or guidelines from the American Association of Physicists in Medicine or from manufacturers independently exist regarding the maximum dose tolerance for INS devices. Manufacturers recommend not placing the device directly in the field of radiation. Still, considerable dose can be measured to the INS outside of the opening in the radiation aperture. For this reason, the dilemma of how to care for a patient with an identified cancer while having the device in place remains as a difficult one. With a possible decision by the neurosurgeon to maintain the presence of the INS to treat the patient's diagnosed problem, the radiation oncologist must then reconsider the treatment options and contingency plans for such situations. Some of these considerations include; (a) declining to treat the patient altogether at the risk of causing detriment to the device and/or causing injury, (b) treating the patient with the device intact while integrating non-standard geometries to avoid the device entirely, or (c) treating the patient with the device intact with a consideration to modify the dose prescription as a safety margin for unpublished device dose tolerances. The information presented here provides the first study of therapeutic treatment planning effects for radiation oncologists and neurosurgeons when neurostimulators remain implanted in a patient.

We provide this research as the initial step to providing treatment planning computer modeling with phantom and clinical case studies of effects caused by devices in the beam of a particle accelerator. The aim for this grant supported research was to provide insight to such complex issues and motivate

researchers and industry to consider investigational research towards this remaining information given the increasing likelihood of clinical cases involving neuromodulation devices. According to the American Association of Neurological Surgeons (AANS), 16,311 spinal cord stimulators and 13,909 deep brain stimulators were implanted in 2006 alone [18]. Together, the two modalities comprised over 55% of all pain, interventional, and functional procedures conducted by neurosurgeons. To date, more than 85,000 patients have been treated with deep brain stimulation therapy worldwide. The use of stimulators by neurosurgeons has been increasing rapidly. With many of the patients with stimulation devices implanted now getting older and more at risk for developing a cancer, this advancement of neuroscience technology is now a critical issue that radiation oncologists have to adjust to clinically. This research provides the first step in that regard by providing to radiation oncologists measured proof that treatment planning systems are unable to accurately detail the physical processes of scatter and attenuation on computer.

These results are restricted to only Medtronic devices mentioned in this manuscript. Such effects are hypothesized to exist for other implantable neuromodulation devices, but the extent of attenuation and scatter magnitude is currently unknown. No claims or conclusions can be made about the evaluation of devices from other manufacturers.

Acknowledgements

Funding

References

[1] R. North, D. Kidd, M. Zuhurak, C.S. James and D.M. Long, Spinal Cord Stimulation for Chronic, Intractable Pain: Experience Over Two Decades, *Neurosurgery* **32** (1993), 384–395.
[2] K. Kumar, C. Toth, R. Nath and P. Laing, Epidural Spinal Cord Stimulation for Treatment of Chronic Pain – Some Predictors of Success. A 15-year Experience, *Surg Neurol* **50** (1998), 110–121.
[3] J. Devulder, M. De Laat, M. Van Bastalaere and G. Rolly, Spinal Cord Stimulation: a Valuable Treatment for Chronic Failed Back Surgery Patients, *J Pain Symptom Manage* **13** (1997), 296–301.
[4] A. Umemura, J. Jaggi, H. Hurtig, A.D. Siderowf, A. Colcher, M.B. Stern and G.H. Baltuch, Deep Brain Stimulation for Movement Disorders: Morbidity and Mortality in 109 Patients, *J Neurosurg* **98** (2003), 779–784.
[5] U.S. Food and Drug Administration, Center for Devices and Radiological Health: FDA Preliminary Public Health Notification: Possible Malfunction of Electronic Medical Devices Caused By Computed Tomography (CT) scanning, (2008), Letter.
[6] Medtronic website: Our Therapies. http://www.medtronic.com/our-therapies/index.htm, Accessed 11/1/2010.
[7] J. Riley, T. Garcia and T. Guerrero, The Utilization of a 3-Dimensional Non-coplanar Treatment Plan to Avoid Pacemaker Complication, *Med Dos* **29** (2003), 92–96.

[8] P. Gullane, Primary Mandibular Reconstruction: Analysis of 64 Cases and Evaluation of Interface Radiation Dosimetry on Bridging Plates, *Laryngoscope* **101** (1991), 1–24.

[9] F. Hudson, M. Crawley and M. Samarasadera, Radiotherapy Treatment Planning for Patients Fitted with Prostheses, *Br J Radiol* **57** (1984), 603–608.

[10] M. Gossman, J. Seuntjens, M.S. Serban, R.C. Lawson, M.A. Robertson, K.J. Christian, J.P. Lopez and T.W. Justice, Dosimetric Effects Near Implanted Vascular Access Ports: an Examination of External Photon Beam Dose Calculations, *J Appl Clin Med Phys* **10** (2009), 3–15.

[11] M. Gossman, A. Graves-Calhoun and J. Wilkinson, Establishing Radiation Therapy Treatment Planning Effects Involving Implantable Pacemakers and Implantable Cardioverter-defibrillators, *J Appl Clin Med Phys* **11** (2010), 1–13.

[12] G.A. White, U.S. FDA, Center for Devices and Radiological Health, (2008), Letter.

[13] C. Coolens and P. Childs, Calibration of CT Hounsfield Units for Radiotherapy Treatment Planning of Patients with Metallic Hip Prostheses: the Use of the Extended CT-scale, *Phys Med Biol* **48** (2003), 1591–1603.

[14] A. Hebb and A. Poliakov, Imaging of Deep Brain Stimulation Leads Using Extended Hounsfield Unit CT, *Stereotact Funct Neurosurg* **87** (2009), 155–160.

[15] G. Fogliata, E. Nicolin, E. Vanetti, A. Clivio and L. Cozzi, Dosimetric Validation of the Anisotropic Analytical Algorithm for Photon Dose Calculation: Fundamental Characterization in Water, *Phys Med Biol* **51** (2006), 1421–1438.

[16] P. Almond, P. Biggs, B. Coursey, W.F. Hanson, M.S. Huq, R. Nath and D.W.O. Rogers, AAPM's TG-51 Protocol for Clinical Reference Dosimetry of High-energy Photon and Electron Beams, *Med Phys* **26** (1999), 1847–1870.

[17] C. Reft, R. Alecu, I. Das, B.J. Gerbi, P. Keall, E. Lief, B.J. Mijnheer, N. Papanikolaou, C. Sibata and J. Van Dyk, Dosimetric Considerations for Patients with HIP Prosthetics Undergoing Pelvis Irradiation – Report of the AAPM Radiation Therapy Committee Task Group 63, *Med Phys* **30** (2003), 1162–1182.

[18] American Association of Neurological Surgeons: National Neurosurgical Procedure Statistics, (2008).